

The near-infrared radiation background, gravitational wave background and star formation rate of Pop III and Pop II during cosmic reionization

Y. P. Yang^{1,2}, F. Y. Wang^{1,2} and Z. G. Dai^{1,2}

¹ School of Astronomy and Space Science, Nanjing University, Nanjing 210093, China

² Key Laboratory of Modern Astronomy and Astrophysics (Nanjing University), Ministry of Education, Nanjing 210093, China
e-mail: fayinwang@nju.edu.cn

July 11, 2018

ABSTRACT

Context. The transition from Population III (Pop III) to Population II (Pop II) stars plays an important role in the universe history. Due to a huge amount of ionizing photons generated by Pop III stars, they begin to ionize the intergalactic medium (IGM) at the early stage of reionization. Meanwhile, the feedback from reionization and metal enrichment changes the evolution of different populations. The near-infrared radiation background (NIRB) and the background of gravitational waves (SBGWs) from these early stars will provide important information about the transition from Pop III to Pop II stars.

Aims. In this paper, we obtain the NIRB and SBGWs from the early stars, which are constrained by the observation of reionization and star formation rate.

Methods. We study the transition from Pop III to Pop II stars via the star formation model of different population, which takes into account the reionization and the metal enrichment evolution. We calculate the two main metal pollution channels arising from the supernova-driven protogalactic outflows and “genetic channel”. We obtain the SFRs of Pop III and Pop II and their NIRB and SBGWs radiation.

Results. We predict that the upper limit of metallicity in metal-enriched IGM (the galaxies whose polluted via “genetic channel”) reaches $Z_{\text{crit}} = 10^{-3.5} Z_{\odot}$ at $z \sim 13$ ($z \sim 11$), which is consistent with our star formation model. We constrain on the SFR of Pop III stars from the observation of reionization. The peak intensity of NIRB is about $0.03 - 0.2 \text{ nWm}^{-2}\text{sr}^{-1}$ at $\sim 1 \mu\text{m}$ for $z > 6$. The prediction of NIRB signal is consistent with the metallicity evolution. We also obtain the gravitational wave background from the black holes formed by these early stars. The predicted gravitational wave background has a peak amplitude of $\Omega_{\text{GW}} \simeq 8 \times 10^{-9}$ at $\nu = 158 \text{ Hz}$ for Pop II star remnants. However, the background generated by Pop III.2 stars is much less than Pop II stars, with a peak amplitude of $\Omega_{\text{GW}} \simeq 1.2 \times 10^{-11}$ at $\nu = 28 \text{ Hz}$. The background of Pop III.1 shifts to lower frequencies, and the amplitude of Ω_{GW} for Pop III.1 stars shows a minimum value at $\nu \simeq 10 \text{ Hz}$, due to the lack of gravitational wave signals from the stars with $140 M_{\odot} < M_{*} < 260 M_{\odot}$.

Key words. cosmology: theory – diffuse background – intergalactic medium – gravitational waves – stars: early type

1. INTRODUCTION

The first stars, known as Population III (Pop III), form at the end of the cosmic dark age and open the reionization era. Pop III stars can have different characteristics compared to Pop I/II stars. Some authors have stated that Pop III can be very massive, on the order of $500 - 600 M_{\odot}$ (Abel et al. 2002; Omukai & Palla 2001, 2003; Bromm & Loeb 2004), while others have claimed that the masses are lower, on the order of $30 - 60 M_{\odot}$ or $10 M_{\odot}$ (Hosokawa et al. 2011, 2012; Stacy et al. 2012). The initial conditions for Pop III star formation are entirely determined by the basic parameters of the cosmology (Tegmark et al. 1997; Yoshida et al. 2003; Bromm et al. 2009). According to the popular “bottom-up” hierarchical structure formation in the standard cold dark-matter (CDM) model, the first stars form in a sufficient amount of cold dense gas in a dark matter halo with mass $\gtrsim 10^6 \sim 10^8 M_{\odot}$, which collapses at redshift $z \sim 20 - 30$ (Bromm et al. 1999, 2002; Abel et al. 2002). At first, these stars contain no elements heavier than helium, viz., metal free, so-called Pop III.1. The second generations of stars originate from the environment influenced by earlier star formation, defined

as Pop III.2, which exist in a pre-ionized region and are affected by previous generations of stellar radiation due to photo-ionization of ambient neutral hydrogen of Pop III.1 stars. Because of supernova (SN) explosions and stellar winds, heavier elements are introduced into the intergalactic medium (IGM), gradually increasing its metallicity. On the other hand, some new galaxies inherit the metals from their low-mass progenitors. After the metal elements enriching to a certain threshold Z_{crit} , the Pop I/II stars form (Bromm et al. 2001; Bromm & Loeb 2003; Schneider et al. 2002, 2006a; Mackey et al. 2003).

There has not been any direct observation of Pop III stars. Fortunately, there are some observations to constrain the early stellar population and reionization, e.g. the near-infrared radiation background (NIRB), Gunn-Peterson trough (Fan et al. 2006) and the background of gravitational waves (Marassi et al. 2009; Pereira & Miranda 2010). NIRB contains some important information of early universe, which arises from accumulated emission from the early galaxy populations with a large range of redshifts. Because photons lose energy in cosmic expansion, the optical and UV radiation from the early stars during reionization should leave a signature in the ex-

tragalactic background light at NIR bands with wavelength less than a few micrometers. Although most high-redshift galaxies are below the limiting magnitude of current detectors, we could observe their redshifted cumulative spectrum, which would be present in any background emission in the NIR band (Barkana & Loeb 2000; Salvaterra & Ferrara 2006; Wyithe & Loeb 2006; Kistler et al. 2009; Bouwens et al. 2010; Robertson et al. 2010; Fernandez & Shull 2011; Muñoz & Loeb 2011). On the other hand, since Pop II galaxies at $z \sim 6$ are already observed with Hubble Space Telescope (HST) and will be in a short time studied in great details with James Webb Space Telescope (JWST), by studying the NIRB intensity, we can find many properties of the early stars, such as the star formation rate of high-redshift stars whose photons are redshifted, the clustering properties (by studying the anisotropy power spectrum of the NIRB), the classification of Pop III stars (by studying the number of the Lyman alpha bumps), the transition from Pop III to Pop II stars (by studying the evolution of Lyman bumps), the reionization and metal enrichment (as we discussed in this paper). However, determining the contribution of these early stars at high redshifts from observations is a hard task. There are two reasons: first, low redshift and very faint galaxies make a significant contribution to NIRB, which is not measured accurately. Second, the extragalactic NIRB is hard to distinguish from the brighter zodiacal foregrounds in the local matter, (e.g. interplanetary dust within the solar system), and the stars and the interstellar medium (ISM) of our Galaxy (Hauser & Dwek 2001; Kashlinsky 2005), which is two to three orders of magnitude larger than $10 \text{ nWm}^{-2}\text{sr}^{-1}$. Recent works suggest that the intensity of NIRB cannot be larger than a few tenths $\text{nWm}^{-2}\text{sr}^{-1}$ (Kneiske et al. 2004; Stecker et al. 2006; Franceschini et al. 2008; Gilmore et al. 2009, 2012; Finke et al. 2010; Kneiske & Dole 2010; Inoue et al. 2013). Except for mean intensity, the anisotropy power spectrum of NIRB could provide direct information of these early stars (Cooray et al. 2004; Kashlinsky et al. 2004; Fernandez et al. 2010; Cooray et al. 2012a). The Pop III epoch contains less projected volume than the ordinary galaxy populations (e.g. Pop II stars), leading to larger relative fluctuations, and their anisotropy power spectrum represents the clustering behavior of sources in the IR regime. However, for the ordinary galaxies (containing Pop II stars), their angular power spectrum is nearly a power law over a wide range of angular scales (Cooray et al. 2004, 2012a).

The UV photons ($\lambda \sim 1000\text{\AA}$) produced at $z = 9$ during reionization will be redshifted to the NIR band with wavelength $\lambda \sim 1\mu\text{m}$. Thus the NIRB would depend on the evolution of the early stars during reionization. So far, many works have obtained some information about reionization, e.g. the optical depth for electron scattering, the end of reionization redshift, and the escape fraction of ionizing photons, which can be used to constrain the SFRs of the early stars (Yu et al. 2012; Wang 2013), and further constrain the intensity of NIRB and SBGWs. Recently, there are many studies to calculate the contribution of stars and galaxies responsible for reionization and NIRB (Kashlinsky et al. 2002; Santos et al. 2002; Salvaterra & Ferrara 2003; Cooray & Yoshida 2004; Cooray et al. 2004; Kashlinsky et al. 2004; Kashlinsky 2005; Kashlinsky et al. 2005; Madau & Silk 2005; Magliocchetti et al. 2003; Fernandez & Komatsu 2006; Kashlinsky et al. 2007a; Thompson et al. 2007a,b; Fernandez et al. 2010; Cooray et al. 2012a; Fernandez et al. 2012; Kashlinsky et al. 2012; Fernandez et al. 2013; Fernandez & Zaroubi 2013; Yue et al. 2013). As a crucial part of the entire story of the cosmic history, reionization reflects the transformation of neutral hydrogen in

the IGM into an ionized state, which is due to ionizing photons generated by the early stars and galaxies. In the process of the early star formation, the IGM is enriched with metals that are dispersed by the first SNe and stellar winds. This process might reflect the evolution of the stellar populations, although it is not understood when the transition from Pop III to Pop II takes place, due to an uncertainty in the “critical metallicity” Z_{crit} (Bromm et al. 2001; Jappsen et al. 2009a,b), and the redshift evolution of the IGM metallicity (Barlow & Tytler 1998; Ferrara et al. 2000; Greif & Bromm 2006) and some other metal pollution channels, e.g. “genetic channel” (Schneider et al. 2006b; Trenti & Stiavelli 2009). With more Pop II star forming (although fewer ionizing photons per stellar), there are more ionizing photons to ionize the IGM, and the ionized bubbles gradually overlap, allowing the mean free path of ionizing photons to increase rapidly. The average volume fraction of ionized hydrogen in IGM increase rapidly. At last the entire universe is almost completely ionized (Barkana & Loeb 2001; Robertson et al. 2010; Bromm 2013).

In this paper, We consider two main channels of metals pollution: the supernova-driven protogalactic outflows (Ferrara et al. 2000; Furlanetto & Loeb 2005) and the “genetic channel” (Schneider et al. 2006b; Trenti & Stiavelli 2009). The former assumed that metals are enriched via superbubbles resulting from supernova explosion in protogalaxies, and the latter suggested that the new galaxies inherit metals from the lower mass progenitor galaxies. Moreover, we constrain the SFR through the observations and reionization, e.g. optical depth for electron scattering as measured by WMAP and Planck, and the redshift of the end of reionization with a possible range from 5 to 10. During reionization, the metal elements enrich in IGM. Pop III.1 stars originate from a freshly collapsed halo, and Pop III.2 stars exist in a pre-ionized metal-free region and they form via hydrogen deuteride cooling. Pop II stars originate from the dark matter halos that have been polluted by metal enrichment. Thus the SFRs of these early stars would depend on the the hydrogen reionization fraction and pristine fraction (Greif & Bromm 2006; Wang et al. 2009; de Souza et al. 2011). Following Fernandez & Komatsu (2006), this NIRB consists of several contributions: the continuum emission from stars themselves, the series of recombination lines, the free-free and free-bound continuum emission from ionized gas or nebula, and the two-photon emission. Based on the constraint on the SFRs of the early stars, we can obtain the contribution of the first stars to the high-redshift NIRB during reionization, which is lower than the current observation (the total luminosity $1 \sim 10 \text{ nWm}^{-2}\text{sr}^{-1}$) (Santos et al. 2002; Salvaterra & Ferrara 2003; Cooray & Yoshida 2004; Kneiske et al. 2004; Kashlinsky et al. 2005; Stecker et al. 2006; Kashlinsky et al. 2007a; Franceschini et al. 2008; Gilmore et al. 2009; Finke et al. 2010; Kneiske & Dole 2010; Gilmore et al. 2012; Kashlinsky et al. 2012; Inoue et al. 2013), due to the foreground pollution. On the other hand, as pointed out by Fernandez & Zaroubi (2013), the Lyman α emission from Pop III stars at high redshift could result in “bump” in spectrum of NIRB. This shape of Lyman α “bump” is determined by the transition from Pop III to Pop II stars.

In addition, these early stars are predicted to collapse into black holes (except in the mass range $140 - 260 M_{\odot}$, which die as pair-instability supernova (PISN) (Heger & Woosley 2002)), and expected to be the sources of the stochastic background of gravitational waves (SBGWs) (Schneider et al. 2000; Buonanno et al. 2005; Sandick et al. 2006; Suwa et al. 2007; Marassi et al. 2009; Pereira & Miranda 2010). Based on the SFRs, we calculate the

SBGWs that were produced by these early stars, including Pop II, Pop III.2 and Pop III.1 stars. At present, some gravitational wave interferometers are operating in the frequency of 10 – 3000 Hz, e.g. VIRGO, Laser Interferometer Gravitational-Wave Observatory (LIGO). In the future, next-generation gravitational wave detection will open a lower frequency window, e.g. Laser Interferometer Space Antenna (LISA) covering the frequency range 10^{-4} – 0.1 Hz, and Big Bang Observer (BBO) operating in the range 0.01 – 10 Hz. The signals of gravitational waves will open a new window for the study of the cosmic transition from Pop III to Pop II stars.

The structure of this paper is organized as follows. In Section 2, we outline the stellar models, including the properties of distinct populations and their SFRs during the era of reionization. In Section 3, we give our reionization model by considering the transition from Pop III to Pop II. In Section 4, we calculate the spectrum of NIRB, which is contributed by the early stars before the end of reionization. In Section 5, the gravitational wave spectra produced by Pop III and Pop II stars are presented. In Section 6, discussions and conclusions are given. In the whole paper, we assume a flat Λ CDM model with $\Omega_m = 0.27$, $\Omega_\Lambda = 0.73$, and $H_0 = 71 \text{ km s}^{-1} \text{ Mpc}^{-1}$.

2. THE STELLAR MODELS

In this section, we consider the emissions from early stars during reionization. Following [Fernandez & Komatsu \(2006\)](#), we calculate the emission from two stellar populations. First, Pop III stars can be divided into the first generation stars (Pop III.1), which their formation only depends on initial conditions of the early universe, and the second generation stars (Pop III.2), which exist in a pre-ionized region and are affected by previous generations of stellar radiation due to photo-ionization of ambient neutral hydrogen of Pop III.1 stars. They form via hydrogen deuteride cooling ([Johnson & Bromm 2006](#)) with less masses and extremely poor metallicity $Z \lesssim 10^{-3.5} Z_\odot$. In the hydrogen deuteride cooling process, the gas temperature would reach that of the cosmic microwave background (CMB) within a Hubble time. When the gas temperature reaches the CMB limit, the Pop III.2 stars with typical masses $\sim 40 M_\odot$ form, which are smaller than the typical mass of Pop III.1 stars. For simplification, we assume that the Pop III.2 stars have a lower-mass distribution, but have the approximate properties of the Pop III.1 stars ([Ohkubo et al. 2009](#)), including the intrinsic bolometric luminosity, the effective temperature, the main-sequence lifetime, and the time-averaged hydrogen photoionization rate. Second, the Pop II stars, as metal-poor stars with metallicity $Z = 1/50 Z_\odot$, form in clouds that can undergo metal and dust cooling. The clouds are able to fragment into smaller masses, leading to typical masses less than those of Pop III stars.

2.1. Pop III & Pop II

We adopt the similar initial mass function (IMF) as same as [Cooray et al. \(2012a\)](#) for Pop III.1 and Pop II stars. The IMF of Pop III.1 stars is ([Larson 1998](#))

$$f(M_*) \propto M_*^{-1} \left(1 + \frac{M_*}{M_*^C} \right)^{-1.35}, \quad (1)$$

where $M_*^C = 250 M_\odot$, and the mass range is from 5 to 500 M_\odot . For Pop II stars, we adopt the IMF given by [Salpeter \(1955\)](#)

$$f(M_*) \propto M_*^{-2.35}, \quad (2)$$

with the mass range from 5 to 150 M_\odot . As pointed out by [Johnson & Bromm \(2006\)](#), we use an intermediate stellar IMF between Pop III.1 and Pop II for Pop III.2 stars. We adopt the IMF given by [Larson \(1998\)](#) with $M_*^C = 150 M_\odot$, and the mass range is from 5 to 250 M_\odot . So the mean mass of Pop III.2 is $\sim 40 M_\odot$, which is consistent with the typical mass given by [Yoshida et al. \(2007\)](#) and [Hosokawa et al. \(2011\)](#). The normalization is given by

$$\int_{M_{*,\min}}^{M_{*,\max}} dM_* f(M_*) = 1. \quad (3)$$

The mean stellar mass of one population is

$$\bar{M}_* = \int_{M_{*,\min}}^{M_{*,\max}} dM_* M_* f(M_*). \quad (4)$$

Here we use the results from [Lejeune & Schaerer \(2001\)](#) and [Schaerer \(2002\)](#) to calculate the main stellar parameters, such as the intrinsic bolometric luminosity $L_*^{\text{bol}}(M_*)$, the effective temperature $T_*^{\text{eff}}(M_*)$, the main-sequence lifetime $\tau_*(M_*)$, and the time-averaged hydrogen photoionization rate $\bar{R}_{\text{HI}}(M_*)$. At first we define $x = \log_{10}(M_*/M_\odot)$.

For Pop III stars (Pop III.1 and Pop III.2), the parameters are given by

$$\begin{aligned} \log_{10}(L_*^{\text{bol}}/L_\odot) &= 0.4568 + 3.897x - 0.5297x^2, \\ \log_{10}(T_*^{\text{eff}}/\text{K}) &= 3.639 + 1.501x - 0.5561x^2 + 0.07005x^3, \\ \log_{10}(\tau_*/\text{yr}) &= 9.785 - 3.759x + 1.413x^2 - 0.186x^3, \\ \log_{10}(\bar{R}_{\text{HI}}/\text{s}^{-1}) &= \begin{cases} 39.29 + 8.55x & (5M_\odot \leq M_* \leq 9M_\odot) \\ 43.61 + 4.90x - 0.83x^2 & (9M_\odot < M_* \leq 500M_\odot) \end{cases} \end{aligned} \quad (5)$$

For Pop II stars, the parameters become

$$\begin{aligned} \log_{10}(L_*^{\text{bol}}/L_\odot) &= 0.138 + 4.28x - 0.653x^2, \\ \log_{10}(T_*^{\text{eff}}/\text{K}) &= 3.92 + 0.704x - 0.138x^2, \\ \log_{10}(\tau_*/\text{yr}) &= 9.59 - 2.79x + 0.63x^2, \\ \log_{10}(\bar{R}_{\text{HI}}/\text{s}^{-1}) &= 27.80 + 30.68x - 14.80x^2 + 2.50x^3. \end{aligned} \quad (6)$$

This stellar model gives the number of ionizing photons emitted per stellar baryon

$$\eta_{\text{ion}} \approx \left\langle \frac{\bar{R}_{\text{HI}}(M_*) \tau_{\text{eff}}(M_*)}{M_*} \right\rangle \frac{m_p}{1 - Y}, \quad (7)$$

where m_p is the proton mass, $Y = 0.25$ is the mass fraction of helium, and $\tau_{\text{eff}}(M_*)$ is the effective stellar lifetime, given by Eq (51) in Section 4. The effective stellar lifetime τ_{eff} may be less than the real lifetime τ_* , because some low-mass stars are still not dead.

2.2. The star formation rate

Following [Greif & Bromm \(2006\)](#), we consider that the Pop III.1 stars form in the minihalos with the minimum virial temperature $T_{\text{vir}} \approx 10^3 \text{ K}$. Pop III.2 stars form in metal-free halos above $T_{\text{vir}} = 10^4 \text{ K}$ via HD cooling. When star formation begins, a sufficient amount of cold dense gas accumulating in a dark matter halo is needed. Because of the collapse of the dark matter halos, the baryonic gas becomes virial equilibrium with the dynamically-dominant dark matter halos,

$$\frac{GM_h}{R_{\text{vir}}} \sim v_{\text{vir}}^2, \quad (8)$$

where M_h is the dark matter halo mass, R_{vir} is the virial radius, and v_{vir} is the virial velocity. The virial radius is (Barkana & Loeb 2001; Bromm 2013)

$$R_{vir} \approx 0.2 \text{ kpc} \left(\frac{M_h}{10^6 M_\odot} \right)^{1/3} \left(\frac{1+z}{10} \right)^{-1} \left(\frac{\Delta_c}{200} \right)^{-1/3}, \quad (9)$$

where $\Delta_c = \rho_{vir}/\rho_b$ is the overdensity after virialization nearly finishes, ρ_{vir} is the virial density of dark matter halos, $\rho_b = \Omega_b \rho_{cr}$ is the baryon mass density of the universe, and $\Delta_c \approx 18\pi^2$ in the Einstein-de Sitter model. The gas heats up resulting from the collapse of the dark matter halo, in which the virial temperature of the gas corresponds to the virial velocity of dark matter halos. So $k_B T_{vir} \sim \mu m_p v_{vir}^2$, which is leading to

$$T_{vir} \approx 10^3 \text{ K} \mu \left(\frac{M_h}{10^6 M_\odot} \right)^{2/3} \left(\frac{1+z}{10} \right), \quad (10)$$

where $\mu = 1.2, 0.6$ is the mean molecular weight for neutral and ionized primordial gas, respectively. For a dark matter halo with mass of $10^6 M_\odot$, the virial temperature in this minihalo is $\sim 10^3 \text{ K}$, which is below the threshold $\sim 10^4 \text{ K}$ of the cooling temperature of atomic hydrogen, so that the gas is unable to cool, resulting in no star formation. The gas would simply persist in hydrostatic equilibrium. However, the cooling in such a low-temperature primordial gas could rely on molecular hydrogen (H_2) instead. The main formation channel is the sequence: $\text{H} + \text{e}^- \rightarrow \text{H}^- + \gamma$, followed by $\text{H}^- + \text{H} \rightarrow \text{H}_2 + \text{e}^-$ (Bromm 2013). At last, the evolution of gas inside minihalos, driven by H_2 cooling, leads to the formation of Pop III.1 stars with typical masses $\sim 100 M_\odot$. After the Pop III.1 star formation, the composition of the primordial gas becomes different, and the cooling process would be more complicated. The hydrogen deuteride (HD) molecule provides an additional cooling channel. For such a dark matter halo with mass of $\geq 10^8 M_\odot$, the cooling of HD would be efficient with temperature $\sim 10^4 \text{ K}$, leading to the formation of Pop III.2 with the typical masses $\sim 40 M_\odot$.

In order to obtain the SFRs of the early stars, we consider a semi-analytic approach by using the collapse fraction function of a dark matter halo. The famous one is the Press-Schechter formalism providing a way to calculate the abundance of the mass of dark matter halos (Press & Schechter 1974). For a given power spectrum $P(k) \propto |\delta_k|^2$, we adopt the matter power of Komatsu et al. (2009). The Gaussian variance of the fluctuations on the mass-scale M_h is

$$\sigma_{M_h}^2 = \frac{1}{2\pi^2} \int_0^\infty P(k) W(k, R_h), \quad (11)$$

where $M_h = (4/3)\pi\rho_{vir}R_h^3$ and $W(k, R_h)$ is a top-hat filter function

$$W = \frac{3}{(kR_h)^3} [\sin(kR_h) - (kR_h) \cos(kR_h)]. \quad (12)$$

The comoving number density of dark matter halos per unit mass could be given by Press & Schechter (1974) formalism

$$\frac{dn_{PS}}{dM_h} = \frac{\Omega_m \rho_{cr}}{M_h^2} \sqrt{\frac{2}{\pi}} \frac{\delta_c}{\sigma_{M_h} D(z)} e^{-\delta_c^2 / 2\sigma_{M_h}^2 D^2(z)} \frac{-d \ln \sigma_{M_h}}{d \ln M_h}, \quad (13)$$

where the critical density of the universe is $\rho_{cr} = 1.8785 \times 10^{-29} h^2 \text{ g cm}^{-3}$, and $\delta_c = \delta\rho/\rho = 1.686$ is the critical overdensity for a spherical perturbation. For the ΛCDM model, the growth factor is given by $D(z) = g(z)/(1+z)g(0)$, where

$$g(z) = \frac{(5/2)\Omega_m(z)}{\Omega_m^{4/7} - \Omega_\Lambda + (1 + \Omega_m(z)/2)(1 + \Omega_\Lambda(z)/70)}, \quad (14)$$

with

$$\Omega_m(z) = \frac{\Omega_m(1+z)^3}{\Omega_m(1+z)^3 + \Omega_\Lambda}, \quad (15)$$

$$\Omega_\Lambda(z) = \frac{\Omega_\Lambda}{\Omega_m(1+z)^3 + \Omega_\Lambda}. \quad (16)$$

A fraction of mass in the universe collapsing into halos with the mass more massive than $M_{h,min}$, referred to as the collapse fraction, is written as

$$F_{col} = \frac{1}{\rho_m} \int_{M_{h,min}}^{M_{h,max}} M_h n_{PS}(M_h, z) dM_h, \quad (17)$$

where $\rho_m = \Omega_m \rho_{cr}$ is the matter density of the universe, and $n_{PS}(M_h, z)$ is obtained by the PS formalism. $M_{h,min}$ and $M_{h,max}$ are determined by the virial temperature. Thus the preliminary SFR is given by (Greif & Bromm 2006)

$$\psi(z) = f_* \rho_m \frac{\Omega_b}{\Omega_m} \left| \frac{dF_{col}}{dz} \right| \left| \frac{dz}{dt} \right|, \quad (18)$$

where f_* is the star formation efficiency.

The transition from Pop III to Pop II stars is dependent on the evolution of metallicity. Here, we consider two channel of metal pollution: supernova-driven protogalactic outflows (Ferrara et al. 2000; Furlanetto & Loeb 2005) and the “genetic channel” (Schneider et al. 2006b; Trenti & Stiavelli 2009). At first, we consider that metals are enriched via supernova-driven protogalactic outflows. For a protogalaxy within a dark matter halo, metals are blow out by superbubbles (SBs) resulting from supernova explosion. According to Ferrara & Tolstoy (2000), the condition of blowout is that the blowout velocity v_b should be larger than the escape velocity v_e , which gives the fraction of the mechanical energy of superbubble that can blowout. The efficiency of the metal escape produced by SNe is close to unity when blowout does take place (MacLow & Ferrara 1999). If a primordial galaxy has an exponentially stratified density distribution $\rho \propto \exp(-z/H)$, then the shock wave from SN explosion initially is decelerated by ISM and subsequently accelerated due to blowout in a lower density environment and continued SB luminosity. The velocity of shock wave has a minimum at $z = 3H$, which is defined as the blowout velocity. It is given by (Ferrara & Tolstoy 2000)

$$v_b \approx 2.7 \left(\frac{L}{\mu m_p n H^2} \right)^{1/3}, \quad (19)$$

where L is the mechanical luminosity of SBs, n is the number density of a uniform ambient medium of protogalaxies, and H is taken to be a free parameter. For ISM parameters $n = 0.5 \text{ cm}^{-3}$, $\mu = 1.25$, blowout occurs if $v_b > v_e$. Thus, the critical mechanical luminosity should be

$$L_c = 0.05 \mu m_p n H^2 \left(\frac{GM_h}{R_h} \right)^{3/2}. \quad (20)$$

The total mechanical luminosity L_t must be larger than L_c when blowout occurs. Here we assume the escape velocity is equal to the circular velocity of the halo $v_e \approx v_c = (GM_h/R_h)^{1/2}$. The total mechanical luminosity of SB in a galaxy could given by (Ferrara 1998)

$$L_t = \varepsilon_{SN} v_f f_b \frac{\Omega_b}{\Omega_m} \frac{M_h}{t_{ff}(z)}, \quad (21)$$

where $\varepsilon_{SN} = 10^{51}$ erg is the characteristic energy of a SN, the cooling fraction of baryons $f_b \approx 1$ in the halo $10^{4.3} \text{K} < T_{vir} < 10^{5.7} \text{K}$ (Madau et al. 2001), and f_* is the star formation efficiency. $t_{ff}(z) = (4\pi G \rho_m(z))^{-1/2}$ is the free fall time of dark matter halo. A typical mechanical luminosity is $L_t \approx 2.3 \times 10^{38} \text{erg s}^{-1}$ for $M_h = 10^8 M_\odot$ and $z = 10$. The mass in stars per SN event ν^{-1} , which is given by

$$\nu^{-1} = \frac{\int_{M_{*,min}}^{M_{*,max}} M_* f(M_*) dM_*}{\int_{8M_\odot}^{M_{*,max}} f(M_*) dM_*}. \quad (22)$$

Here we assume the lowest mass of SN progenitors is $8M_\odot$. Eq (21) gives the total mechanical luminosity. However, only a fraction of the mechanical luminosity could blowout from galaxies, because the SNe might be occur in different regions in one galaxy, and some superbubbles with low mechanical luminosity could not blowout in certain regions. Thus we calculate the efficiency of blowout following Ferrara et al. (2000). Pop III.1 stars are formed in minihalos, and recent simulation (Bromm et al. 2009) implies that a minihalo only contains one Pop III.1 star. Thus the star formation may be confined to a small region, leading to SN explosions in the formation of a single superbubble. In this case, the single superbubble is likely to blowout $L_t > L_c$ and the fraction of the mechanical energy that could blowout is $\eta_B \approx 1$. For larger galaxies where Pop III.2 and Pop II stars formed (Bromm 2013), the SNe would occur in different OB associations, which are more widely distributed within galaxies. The luminosity function of OB association is approximated by (Oey & Clarke 1997; Portegies Zwart et al. 2010)

$$\frac{dN_{OB}}{dL_{OB}} \propto \frac{dN_{OB}}{dN} = KN^{-2}, \quad (1 \leq N \leq N_{max}), \quad (23)$$

where N is the number of SN in a cluster. The probability to have N SNe in one OB association is $p \approx N^{-2}$, and the average probability is $\bar{p} \approx 1/N_{max}$. The average number of SN per OB association $\bar{N}_{SN} \approx N_{tot}/N_{max}$. The total number of supernovae could be given by $N_{tot} \approx f_* f_b (\Omega_b/\Omega_m) M_h / t_{ff}(z)$. The total number of OB associations is $K \sim N_{max}$. The mechanical luminosity of an OB association is $L_{OB} = N \varepsilon_{SN} / t_{OB}$, where $t_{OB} = 40 \text{ Myr}$ is the time at which the lowest mass SN progenitor expires $\sim 8M_\odot$. The total mechanical luminosity could be given by

$$L_t(z) = \int_1^{N_{max}} L_{OB} dN_{OB} = N_{max} \frac{\varepsilon_{SN}}{t_{OB}} \ln N_{max} \approx N_{tot} \frac{\varepsilon_{SN}}{t_{OB}}. \quad (24)$$

The first total mechanical luminosity given by Eq(21) is calculated via the star formation rate of a proto-galaxy, which is related to the mass of the dark matter halo. The second total mechanical luminosity given by Eq(24) is to obtain the efficiency of blowout, which is related to the number of SNe in a cluster. Physically, the latter mechanical luminosity must be equal to the former. This relation between the maximum number of SN and the total number of SN is approximately

$$N_{tot} = N_{max} \ln N_{max}. \quad (25)$$

The above equation describes the dependence of the total number of SN N_{tot} as a function of the maximum number of SN in a cluster, and we assume that the maximum possible number of SN in a cluster is $N_{max} \lesssim 500$, which is consistent with the Monte Carlo simulation of Ferrara et al. (2000). We find that Eq(25) could be applied to the case of Pop III.1 stars in minihalos

with $M_h \sim 10^6 M_\odot$. Similarly, the effective mechanical luminosity leading to blowout is

$$L_b(z, > L_c) = N_{max} \frac{\varepsilon_{SN}}{t_{OB}} \ln \frac{N_{max}}{N_c}, \quad (26)$$

where $N_c = L_c t_{OB} / \varepsilon_{SN}$ is the number of SN in a cluster with mechanical luminosity. Thus the fraction of the mechanical energy that could blowout is defined as (Ferrara et al. 2000)

$$\eta_B \equiv \frac{L_b}{L_t} = \frac{\ln(N_{max}/N_c)}{\ln N_{max}}. \quad (27)$$

After the shock wave of SBs propagates to IGM, the metal bubble would be enriched to a larger zone due to the lower density of IGM. The outflow will be confined by the pressure of IGM, which determines the radius of the metal bubble. The shell growth stalls when $P_i = P_0$, where P_0 is the IGM pressure in the surroundings of the galaxy as $P_0 = n(z) k_B T$, where $n(z)$ is the average baryon number density of the cosmology, and the gas of IGM is heated to $T \approx 2 \times 10^4 \text{K}$ by photoionization heating. During the ionized zone overlapping, the SN-driven bubbles would propagate in the photoionization gas. Here we assume that the outflow propagates in ionized zone.

We consider the standard evolution for an adiabatic, pressure-driven superbubble. The growth of the SN shell radius is (Weaver et al. 1977)

$$R = \left(\frac{125}{254}\right)^{1/5} \left(\frac{L t^3}{\mu m_p n_{IGM}}\right)^{1/5}, \quad (28)$$

where $n_{IGM} \approx n(z)$ is the number density of the ambient medium in IGM. The interior pressure is

$$P_i = \frac{7}{(3850\pi)^{2/5}} L^{2/5} (\mu m_p n_{IGM})^{3/5} t^{-4/5}. \quad (29)$$

When the shell growth stalls $P_i = P_0$, we have

$$R_s = \frac{5 \cdot 7^{1/4}}{(550\pi)^{1/2}} L_e^{1/2} (\mu m_p n_{IGM})^{1/4} P_0^{-3/4}, \quad (30)$$

where $L_e = \eta_B L_t$ is the effective mechanical luminosity, which is the fraction available for blowout into IGM. The stall age is

$$t_s = \frac{7^{3/4}}{(550\pi)^{1/2}} (\mu m_p n_{IGM})^{3/4} P_0^{-5/4} L_e^{1/2}. \quad (31)$$

The typical parameters are $R_s \approx 33 \text{ kpc}$ and $t_s \approx 1.5 \text{ Gyr}$ for $M_h = 10^8 M_\odot$ and $z = 10$. If $z \gg 1$ ($\Omega_M \gg \Omega_\Lambda$), the stall redshift is given by (Voit 1996)

$$z_s \approx \left(\sqrt{1+z} - \frac{H_0 t_{st}}{2} \right)^2 - 1, \quad (32)$$

where $t_{st} = t_{ISM} + t_s$. t_{ISM} is the time during which a SN shell spreads through a galaxy, which is much less than the stall age in the IGM. The comoving metal-enrich radius is $R_e \approx (1 + z_s) R_s$. If $t_s \lesssim 1/H_0$, the fraction of space with metals is approximately given by

$$Q'_e(z) \approx \int_{M_{h,min}}^\infty dM_h \frac{4\pi}{3} R_e^3(M_h, z_s) \frac{dn_{PS}}{dM_h}(M_h, z). \quad (33)$$

This equation could be well approximate if the metal-enriched bubble did not overlap and the expanding time is much less than the Hubble time $H^{-1}(z)$. If the protogalaxies are randomly distributed, then the filling factor would be $p'_e(z) = 1 - \exp[-Q'_e(z)]$.

In fact, due to clustering, some new halos form in the metal-enriched regions. The fraction of space with metals should be corrected by an excess probability that two galaxies are located near each other, viz, the galaxy two-point correlation function $\xi_{gg}(R_e) = b_0 b_m \xi_{hh}(R_e)$ (Furlanetto & Loeb 2005), where ξ_{hh} is the correlation function of dark matter halo (e.g. Greif & Bromm (2006)), $b_0 \simeq b(M_{h,min})$ is the bias of the newly formed galaxies and b_m is the bias of the metal enriched regions, which is given by

$$b_m = \frac{\int dM_h (4\pi/3) \rho R_e^3 b(m) (dn_{PS}/dM_h)}{\int dM_h M_h (dn_{PS}/dM_h)}. \quad (34)$$

Thus, the probability that a new halo lies within metal-enriched region is then approximately given by

$$Q_e = Q'_e [1 + \xi_{gg}(R_e)] \quad (35)$$

Finally, the filling factor would be $p_e(z) = 1 - \exp[-Q_e(z)]$ after assuming the wind hosts are randomly.

On the other hand, the metal enrichment of galaxies can proceed via “genetic channel” (Schneider et al. 2006b), that is, metals are enriched via the merger of the lower mass progenitors, rather than through outflows from neighbours. Here, we calculate the probability $f_{old}(z)$ that a new collapsing halos accreting onto some old halos via Extended Press-Schechter model (the Appendix of Furlanetto & Loeb (2005)), which is

$$f_{old}(z) = \frac{\int_{2M_{h,min}}^{\infty} dM_h M_h (dn_{PS}/dM_h) F(< M_{h,min}, z_h | M_h, z)}{\int_{M_{h,min}}^{\infty} dM_h M_h (dn_{PS}/dM_h) F(< M_{h,min}, z_h | M_h, z)}, \quad (36)$$

where the factor 2 is attributed to the assumption that a parent halo with a mass $M_h < 2M_{h,min}$ would be included in the new halo component, and the fraction of the accreted mass in a halo with a mass M_h at redshift z is

$$F(< M_{h,min}, z_h | M_h, z) = \text{erf} \left(\frac{\delta_c(z_h) - \delta_c(z)}{\sqrt{2(\sigma_{M_{h,min}}^2 - \sigma_{M_h}^2)}} \right), \quad (37)$$

where z_h corresponds to some earlier time when a parent halo with a mass ($< M_{h,min}$) formed, which is fixed by the dynamic time within a galaxy (Furlanetto & Loeb 2005). After a halo merging a mass above $M_{h,min}$, it would most likely form Pop II stars. Thus, the probability $p_{gc}(z)$ that a dark matter halo did not inherit any metals from its progenitor is $p_{gc}(z) \simeq 1 - f_{old}(z)$.

In Figure 1, the solid curve corresponds to the evolution of the pristine fraction $p_{pris}(z) = 1 - p_e(z)$, and the dashed curve corresponds to the evolution of $p_{gc}(z)$. We find that the metals of IGM begin to be significantly enriched via supernova-driven protogalactic outflows at $z \sim 10$. However, due to $p_{gc}(z) \sim 0.2 - 0.6$ during a large range redshift, the metal enrichment of galaxies is still dominated by “genetic channel” at $z \gtrsim 6$.

Since the Pop III stars generate many ionizing photons, the ionized bubbles would be photoheated to $\sim 10^4 \text{K}$, which prevent the ionized gas to collapse fresh stars. Thus, the formation of Pop III.1 stars is suppressed by a factor being equal to the volume filling fraction of ionized regions $Q_{ion}(z)$, which is discussed in the next section. The SFR of Pop III.1 stars is given by

$$\begin{aligned} \psi_{III.1}(z) &= f_{*,III.1} \rho_m \frac{\Omega_b}{\Omega_m} (1 - p_e(z)) p_{gc}(z) \\ &\times (1 - Q_{ion}(z)) \left| \frac{dF_{coll}}{dz} \right|_{T_{vir}=10^3 \text{K}} \left| \frac{dz}{dt} \right|. \end{aligned} \quad (38)$$

As pointed out by Johnson & Bromm (2006), the free electrons can boost the production of H_2 , leading to a lower temperature where the HD can be cooled. These stars, originating from metal-free gas and cooling via HD channel, would be less massive than Pop III.1 stars. The formation of Pop III.2 stars requires an increased abundance of free electrons. Here we consider two main pathways toward Pop III.2 (Bromm 2013). The first one results from the photo-ionization of ambient neutral hydrogen of Pop III.1 stars, and the non-equilibrium recombination leads to a boosted abundance of H_2 and HD after the Pop III stars have died (Yoshida et al. 2007). In order to prevent pre-enrichment of the gas, these Pop III stars ($260 < m < 500 M_\odot$) have to directly collapse to black holes, the number fraction of which is $f_n = \int_{260 M_\odot}^{500 M_\odot} dM_* f(M_*) \simeq 6 \times 10^{-2}$. The second one arises from the collision ionization in shocks that originate from the collapse of metal free gas of more massive dark matter halos with $T_{vir} = 10^4 \text{K}$ (Greif & Bromm 2006). Thus, the SFR of Pop III.2 is

$$\begin{aligned} \psi_{III.2}(z) &= \rho_m \frac{\Omega_b}{\Omega_m} (1 - p_e(z)) p_{gc}(z) (f_{*,III.1} f_n Q_{ion}(z) \\ &\times \left| \frac{dF_{coll}}{dz} \right|_{T_{vir}=10^4 \text{K}} + f_{*,III.2} \left| \frac{dF_{coll}}{dz} \right|_{T_{vir}=10^4 \text{K}}) \left| \frac{dz}{dt} \right|. \end{aligned} \quad (39)$$

In fact, the first term in the above equation is small due to the number of the stars that directly collapse to black hole is very few. For Pop II stars, we assume that they are formed from the metal-enriched dark matter halos with $T_{vir} = 10^4 \text{K}$. The SFR of Pop II is

$$\psi_{II}(z) = f_{*,II} \rho_m \frac{\Omega_b}{\Omega_m} [1 - (1 - p_e(z)) p_{gc}(z)] \left| \frac{dF_{coll}}{dz} \right|_{T_{vir}=10^4 \text{K}} \left| \frac{dz}{dt} \right|. \quad (40)$$

In Eq(38) and Eq(39), the SFRs depend on the hydrogen reionization fraction Q_{ion} that is as a function of redshift z , which is discussed in the next section.

Due to inhomogeneous metal pollution, some regions where the metal enrichment is overlapped have larger metallicity. The upper limit of metal-enriched IGM metallicity in these rich regions could be estimated by

$$Z_{rich}(z) = \frac{y_{II}}{p_e(z) \rho_b} \int_z^\infty \eta_B(M_{h,min}, z') \zeta_e(z') \psi_{II}(z') \left| \frac{dt}{dz'} \right| dz', \quad (41)$$

where the metal yields are $y_{II} = 0.005$ for Pop II, which is consistent with the proposed values in Greif & Bromm (2006), ρ_b is the mean baryon mass density of the universe, $\zeta_e(z) \psi_{II}(z)$ is the SFR of Pop II stars which are polluted via supernova-driven protogalactic outflows, and $\zeta_e(z) = p_e(z)/[1 - (1 - p_e(z)) p_{gc}(z)]$. The metals in the overlapped metal-enriched region are mainly from the Pop II stars which are polluted via SNe, thus we ignore the first contribution of metal enrichment via the SNe of Pop III in this overlap region. On the other hand, we calculate the upper limit of the metallicity of the galaxies whose all progenitors were polluted by “genetic channel”, which is

$$Z_{gc}(z) = \frac{y_{II}}{\rho_{ISM}} \int_z^\infty \kappa_v^3 (1 - \eta_B(M_{h,min}, z')) \zeta_{gc}(z') \psi_{II}(z') \left| \frac{dt}{dz'} \right| dz', \quad (42)$$

where $\zeta_{gc}(z) \psi_{II}(z)$ is the SFR of Pop II stars which are polluted via “genetic channel”, and $\zeta_{gc}(z) = [1 - p_{gc}(z)]/[1 - (1 - p_e(z)) p_{gc}(z)]$. We assume that the mean baryon mass density of ISM is $\rho_{ISM} \simeq 10^{-24} \text{cm}^{-3}$, and the ratio of the mean distance between two galaxies to the scale of a galaxy is $\kappa_v \simeq 100$.

3. THE REIONIZATION

The volume filling fraction of hydrogen ionized regions Q'_{ion} is (Madau et al. 1998)

$$\frac{dQ'_{ion}}{dt} = \frac{f_{esc}}{n_{H,0}} \sum_i \psi_i q_i - \frac{Q'_{ion}}{\bar{t}_{rec}}, \quad (43)$$

where i represents Pop II, Pop III.2 and Pop III.1, f_{esc} is the escape fraction of ionizing photons. In fact, due to clustering, the probability that a fresh halo lies within an hydrogen ionized (shown in Eq(38) and Eq(39)) is

$$Q_{ion} = Q'_{ion} [1 + \xi_{hh}(z)] \quad (44)$$

\bar{t}_{rec} is the volume averaged recombination time, which is given by

$$\bar{t}_{rec} = [C_{HII}(z) \alpha_B^{rec} n_{H,0} (1+z)^3 (1+Y/4X)]^{-1}, \quad (45)$$

where $C_{HII}(z) \equiv \langle n_{HII}^2 \rangle / \langle n_{HII} \rangle^2$ is the clumping factor of ionized hydrogen. We use a simple analytic fit of the form $C_{HII}(z) = 1 + 9[(1+z)/7]^{-2}$ for $z > 6$, and $C_{HII}(z) = 10$ for $z \leq 6$ (Greif & Bromm 2006). We assume that the mass fractions of hydrogen and helium are $X = 0.75$ and $Y = 0.25$, respectively. Thus the mean hydrogen number density at $z = 0$ is given by

$$n_{H,0} = \frac{X \Omega_b \rho_{cr}}{m_p} \approx 1.956 \times 10^{-7} \text{ cm}^{-3}. \quad (46)$$

The number of hydrogen-ionizing photons per stellar mass during stellar lifetime is

$$q_i = \left\langle \frac{\bar{R}_{HI}^i \tau_{eff}^i}{M_*^i} \right\rangle, \quad (47)$$

where i presents Pop II, Pop III.2 and Pop III.1 stars, and $\tau_{eff}(M_*)$ is the effective stellar lifetime, which may be less than τ_* , given by Eq. (51). The optical depth for Thomson scattering determined by the ionization history is

$$\tau = c \sigma_T \int_0^\infty dz' Q_{ion}(z') n_{H,0} (1+z')^3 (1+Y/4X) \frac{dt}{dz'}. \quad (48)$$

In order to constrain our star formation model with fewer parameters, we adopt a fixed optical depth of Thomson scattering $\tau = 0.08$, which is satisfied with the observation of WMAP nine-year data with $\tau = 0.089 \pm 0.014$ (Hinshaw et al. 2013) and the observation of Planck results with $\tau = 0.066 \pm 0.016$ (Ade et al. 2015). The star formation efficiency of Pop II stars is assumed to be $f_{*,II} = 0.01$, which is constrained by the observation of the SFR at $z \sim 5 - 10$ (Bouwens et al. 2012a,b; Schenker et al. 2013). We take the same value of the star formation efficiency $f_{*,III}$ for both Pop III.1 and Pop III.2 and the same value of the escape fraction of ionizing photons for all populations f_{esc} . We assume that stars form from redshift $z_{in} = 30$. Figure 2 shows the three epochs of the cosmic star formation history: the blue line denotes Pop II stars, the black line denotes Pop III.1 stars, and the red line denotes Pop III.2 stars. Because the negative feedback from a star forming in a dark matter halo prevents the formation of other stars in the same halos, leading to Pop III stars have a lower star formation efficiency than Pop II stars, and we set $f_{*,III} \leq f_{*,II}$. For the same optical depth $\tau = 0.08$, we consider three cases: Case A ($f_{*,III} = 0.01$, $f_{esc} = 0.21$), Case B ($f_{*,III} = 0.004$, $f_{esc} = 0.45$) and Case C ($f_{*,III} = 0.002$, $f_{esc} = 0.75$), which are denoted by dashed, solid and dotted lines, respectively.

For the same τ value, a larger value of f_{esc} will result in a lower SFR and a lower value of f_{esc} in a larger SFR. We also find that the SFR of Pop II raising earlier due to the metal pollution via “genetic channel”.

Figure 3 shows the reionization history for three star formation models. The end of reionization is $z_{end} = 5.1, 6.9, 7.2$, corresponding to Case A, B and C, which are denoted by dashed, solid and dotted lines, respectively. We find that larger SFR of Pop III.1 stars causes a larger hydrogen reionization fraction at high redshift, however, lower f_{esc} leads to a later end of reionization. Due to larger SFR of Pop III.1 at high redshift and a huge amount of ionizing photons generated by Pop III.1 stars, the hydrogen reionization fraction Q_{ion} raises at a higher redshift $z \sim 20$ until the SFR of Pop III.1 becoming low at $z \sim 10$. Soon the Pop III.2 and Pop II stars rapidly form, leading to the hydrogen reionization fraction Q_{ion} raising rapidly until the universe completely ionized.

According to Eq (41) and Eq (42), we obtain the evolution of the upper limit of the metallicities in the metal-enriched region of IGM and in the galaxies whose all progenitors were polluted via “genetic channel”, as shown in Figure 4. The upper limit is attributed to the inhomogeneous metal pollution. We predict that: (i) for the metal-enriched region of IGM, the upper limit of the metallicity reaches $Z_{crit} = 10^{-3.5} Z_\odot$ (Bromm et al. 2001; Schneider et al. 2002) at $z \sim 13$; (ii) for the galaxies polluted via “genetic channel”, it reaches the critical value at $z \sim 11$. Pop II stars with low mass formed for $Z \gtrsim Z_{crit}$, which is in good agreement with the star formation model in Figure 2. Note that as shown in Figure 1, the metal enrichment is dominated by “genetic channel”, however, at a certain redshift, the upper limit of the metallicity of the metal-enriched region is larger than that of the galaxies polluted via “genetic channel”. The reason is that the fraction of space with metals is so small that the metallicity would be large, if the Pop II stars that were polluted via SN outflows always form in this metal-enriched region.

4. THE NEAR-INFRARED BACKGROUND

The intensity of the NIRB offers a window of probing the era of reionization. Following Fernandez & Komatsu (2006), we calculate the NIRB from the epoch of reionization. There are several contributions to the emission of NIRB: the continuum emission from stars themselves \bar{L}_ν^* , the series of recombination lines \bar{L}_ν^{line} , the free-free and free-bound continuum emission from the ionized gas or nebula \bar{L}_ν^{cont} , and the two-photon emission $\bar{L}_\nu^{2\gamma}$. For the first stars, one of the remarkable properties is a “bump” in the spectrum of NIRB, which is from the Lyman α emission (Fernandez & Zaroubi 2013). The Lyman α bump would be higher if Pop III stars were more massive and presented at lower redshifts, and it would evolve with the transition from Pop III stars to Pop II stars. For the IGM, the hydrogen density is lower than that of the stellar nebulae. Here we neglect the emission from IGM, because it is only a small part of NIRB (Cooray et al. 2012a). The intensity of the NIRB is given by

$$I_\nu = \frac{c}{4\pi} \int dz \frac{p((1+z)\nu, z)}{H(z)(1+z)}, \quad (49)$$

where the volume emissivity is given by

$$p(\nu, z) = \frac{\psi(z)}{\bar{M}_*} \sum_\alpha \int dM_* f(M_*) \bar{L}_\nu^\alpha(M_*) \tau_{eff}(M_*). \quad (50)$$

The stellar effective lifetime could be approximately given by

$$\tau_{eff}(M_*) = \min[\tau_*(M_*), T_s(z)]. \quad (51)$$

$\bar{L}_\nu^\alpha(M_*)$ is the time-averaged luminosity in the frequency interval $d\nu$ for a radiative process α for stellar or nebular component, which consists of the stellar blackbody emission, as well as the reprocessed nebular emission, such as two-photon emission, recombination line, free-free and free-bound continuum emission. T_s is the time from the formation of the first stars of the universe to the age of the universe at redshift z (Fernandez & Komatsu 2006).

Following Fernandez & Komatsu (2006), we calculate four contributions to the emission of NIRB: (1). The stellar spectrum, which is the Planck function with the Lyman absorption:

$$\bar{L}_\nu(M_*) = \begin{cases} 4\pi R_*^2(M_*) B_\nu(T_*^{eff}(M_*)), & h\nu < 13.6 \text{ eV}, \\ 0, & h\nu \geq 13.6 \text{ eV}, \end{cases} \quad (52)$$

where $B_\nu(T_{eff})$ is the Planck spectrum. R_* is the stellar radius which is determined by the intrinsic bolometric luminosity $L_*^{bol}(M_*)$ and the effective temperature $T_*^{eff}(M_*)$ are given by Eq(5) and Eq(6), respectively; (2). The luminosity of two-photon emission, which is given by

$$\bar{L}_\nu^{2\gamma}(M_*) = \frac{2h\nu}{\nu_{Ly\alpha}}(1 - f_{Ly\alpha})P(\nu/\nu_{Ly\alpha})\bar{R}_{HI}(M_*), \quad (53)$$

where $\nu_{Ly\alpha} = 2465 \text{ THz}$, $f_{Ly\alpha} = 0.64$, $P(y)dy$ is normalized probability of generating one photon via two-photon decay in the range $dy = d\nu/\nu_{Ly\alpha}$ for $y \equiv \nu/\nu_{Ly\alpha} < 1$ (Fernandez & Komatsu 2006); (3). The line luminosity, which is given by

$$\bar{L}_\nu^{line}(M_*) = f_{Ly\alpha} h\nu_{Ly\alpha} \phi(\nu - \nu_{Ly\alpha}) \bar{R}_{HI}(M_*), \quad (54)$$

where $\phi(\nu - \nu_{Ly\alpha})$ is the line profile, which is taken to be a δ -function $\phi(\nu - \nu_{Ly\alpha}) = \delta^D(\nu - \nu_{Ly\alpha})$. Note that the above equation is for the Lyman alpha line only. (4). The free-free and free-bound continuum luminosity, that is

$$\begin{aligned} \bar{L}_\nu^{cont}(M_*) \simeq & 6.8 \times 10^{-38} \frac{T_g^{-1/2}}{\alpha_B^{rec}} \bar{R}_{HI}(M_*) \phi_2(T_g) e^{-h\nu/kT_g} \\ & \times \left[\bar{g}_{ff} + \frac{R_y}{kT_g} \sum_{n=2}^{\infty} \frac{e^{R_y/(kT_g n^2)}}{n^3} g_{fb}(n) \right], \end{aligned} \quad (55)$$

where the case B recombination coefficient is $\alpha_B^{rec} \simeq 2.17 \times 10^{-10} T_g^{-0.7395}$, \bar{g}_{ff} and $g_{fb}(n)$ are the Gaunt factors for free-free and free-bound emission respectively, approximately, $\bar{g}_{ff} \approx 1.1$ and $g_{fb}(n) \approx 1.05$. T_g is the gas temperature, here we assume that $T_g \approx 10^4 \text{ K}$, and the line profile is $\phi_2(10^4 \text{ K}) \approx 1.0$. Then $\bar{R}_{HI}(M_*)$ is given by Eq(5) and Eq(6).

Figure 5 shows the spectra of NIRB at $z > 6$. Case A, B and C are denoted by dashed, solid, dotted lines, respectively. Different color lines denote different contributions to the emission of NIRB. The Lyman α and two-photons emission are dominant. We find that larger value of $f_{*,III}$ leads to larger Lyman α bump and stronger two-photon emission. The mean intensity of NIRB contributed by these early stars during reionization is nearly $\sim 0.03 - 0.2 \text{ nWm}^{-2} \text{ sr}^{-1}$ at $z > 6$. We also plot the contributions of the different stellar populations to NIRB, as shown in Figure 6. The blue, black and red lines denote the NIRB contribution of Pop II, Pop III.1 and Pop III.2, respectively. We find that the component of the Pop III.2 dominates the total NIRB spectra and the two Lyman α bumps ($\sim 1215(1+z)\text{\AA}$) associated to Pop III.2 and Pop III.1 are obvious at $z > 6$. If we can detect the Lyman α bumps, it would reveal many properties of the early stars, such as the star formation rates, redshift distribution and the classification of the Pop III stars.

5. STOCHASTIC BACKGROUND OF GRAVITATIONAL WAVES

In this section, we calculate the SBGWs that are generated by these stars collapse to black holes. The SBGW is mainly dependent on the SFR and IMF of Pop III and Pop II stars. The flux received in gravitational waves is

$$F_\nu(\nu_{obs}) = \int \frac{1}{4\pi d_L^2} \frac{dE_{GW}}{d\nu} \frac{d\nu}{d\nu_{obs}} \psi(z) \frac{f(M_*)}{\bar{M}_*} dM_* dV. \quad (56)$$

where d_L is the luminosity distance, $dE_{GW}/d\nu$ is the specific energy of the source, $\psi(z)$ is the star formation rate, $f(M_*)$ is the IMF of one population, and \bar{M}_* is the mean stellar mass given by Eq(4). As pointed out by Carr (1980), the specific energy flux per frequency is

$$f_\nu(\nu_{obs}) \equiv \frac{1}{4\pi d_L^2} \frac{dE_{GW}}{d\nu} \frac{d\nu}{d\nu_{obs}} = \frac{\pi c^3}{2G} h_{BH}^2, \quad (57)$$

where h_{BH} is the dimensionless gravitational wave amplitude. The flux of gravitation waves would be

$$F_\nu(\nu_{obs}) = \frac{\pi c^3}{2G} h_{BG}^2 \nu_{obs}. \quad (58)$$

The integral dimensionless gravitational wave amplitude produced from all events that stars collapse to black holes is given by (Pereira & Miranda 2010)

$$h_{BG}^2 = \frac{1}{\nu_{obs}} \int h_{BH}^2 \psi(z) \frac{f(M_*)}{\bar{M}_*} dM_* dV. \quad (59)$$

The comoving volume can be expressed as

$$dV = 4\pi d_C^2 \left(\frac{c}{H_0} \right) \left[\Omega_m (1+z)^3 + \Omega_\Lambda \right]^{-1/2} dz. \quad (60)$$

For the case that a star collapse to a black hole, we assume that gravitational waves radiate with an efficiency $\epsilon_{GW} = \Delta E_{GW}/m_r c^2$, where ΔE_{GW} is the total gravitational waves energy and m_r is the mass of black hole. The efficiency $\epsilon_{GW} \lesssim 7 \times 10^{-4}$, if the collapse is axisymmetric (Stark & Piran 1985). The characteristic amplitude is given by (Thorne 1987)

$$h_{BH} \approx 7.4 \times 10^{-20} \epsilon_{GW}^{1/2} \left(\frac{m_r}{M_\odot} \right) \left(\frac{d_L}{1 \text{ Mpc}} \right)^{-1}, \quad (61)$$

and the observed gravitation waves frequency is

$$\nu_{obs} \approx 1.3 \times 10^4 \text{ Hz} \left(\frac{M_\odot}{m_r} \right) (1+z)^{-1}. \quad (62)$$

We consider that the black holes are formed with $M_* > 25 M_\odot$ for Pop II and Pop III. For the stars with $25 < M_* < 140 M_\odot$, the black holes have the same mass of the helium core of their progenitors (Heger & Woosley 2002)

$$m_r = m_{He} = \frac{13}{24} (M_* - 20 M_\odot). \quad (63)$$

In the range $140 < M_* < 260 M_\odot$, the stars are completely disrupted in PISN explosions, leading to no black holes, $m_r = 0$. For $M_* > 260 M_\odot$, these stars would directly collapse to black holes, thus we neglect stellar mass loss and the masses of the black holes are equal to those of the their progenitor stars, $m_r = M_*$. According to Eq (62), the range of frequency is determined by the mass range of IMF after assuming that the largest redshift

of star formation is $z = 30$. For Pop II, the frequency is $\nu_{obs} > 6.4\text{Hz}$; for Pop III.1, the background is shifted to lower frequencies due to the direct collapse for $M_* > 260M_\odot$, $\nu_{obs} > 0.6\text{Hz}$; and for Pop III.2, $\nu_{obs} > 6.4\text{Hz}$, which has the same range as Pop II stars, because the stars with $140 < M_* < 250M_\odot$ were disrupted by PISN.

The gravitational energy density parameter Ω_{GW} is defined as the closure energy density per logarithmic frequency span (Pereira & Miranda 2010)

$$\Omega_{GW} \equiv \frac{1}{\rho_{cr}} \frac{d\rho_{GW}}{d \ln \nu_{obs}} = \frac{4\pi^2}{3H_0^2} \nu_{obs}^2 h_{BG}^2. \quad (64)$$

In Figure 7, Pop II, Pop III.2 and Pop III.1 stars are denoted by blue, red, black lines, respectively. The sensitivity curves of advanced LIGO H1L1, LISA and BBO are denoted by green, orange and purple, respectively (Thrane & Romano 2013), assuming $T = 1\text{yr}$ of the observation. Case A, B and C are denoted by dashed, solid, dotted lines, respectively. The predicted gravitational wave background has a peak amplitude of $\Omega_{GW} \approx 8 \times 10^{-9}$ at $\nu = 158\text{Hz}$ for Pop II star remnants. However, the background generated by Pop III.2 stars is much weaker than Pop II stars, with a peak amplitude of $\Omega_{GW} \approx 1.2 \times 10^{-11}$ at $\nu = 28\text{Hz}$. The background of Pop III.1 shifted to lower frequencies, and the amplitude of Ω_{GW} for Pop III.1 stars shows a minimum value at $\nu_{obs} \approx 10\text{Hz}$, due to the lack of gravitational wave signals from the stars with $140 < M_* < 260M_\odot$. As shown in Figure 7, it is difficult to observe the SBGWs from the early stars for the gravitational wave detectors. However, as shown in Case A, we might have an opportunity to detect the SBGWs signal from Pop III.1 stars at observed frequency $\nu_{obs} \approx 3.5\text{Hz}$, which are twice than the sensitivity of BBO detector.

6. DISCUSSIONS AND CONCLUSIONS

In this paper, we have constructed the star formation history for Pop III and Pop II via the collapse function of dark matter halos. These SFRs, calculated by the collapse fraction function, are self-consistent with the observations of reionization (the reionization optical depth measured by WMAP and Planck, reionization redshift in range from 5 to 10) and NIRB (the total luminosity $1 \sim 10\text{nWm}^{-2}\text{sr}^{-1}$). At first, Pop III stars form from pristine baryonic gas in dark matter halos. Due to the metal enrichment raising in the universe, more and more Pop II stars formed in metal-enriched region. There are two main channels of the metal pollution: the supernova-driven protogalactic outflows (Ferrara et al. 2000; Furlanetto & Loeb 2005) and the “genetic channel” (Schneider et al. 2006b; Trenti & Stiavelli 2009). The former is assumed that the new dark matter halos are formed in the IGM that is enriched with the metals dispersed by the first SNe and stellar winds, and the latter suggests that the new galaxies inherit metals from the lower mass progenitor galaxies. After the metals in the IGM enriching to a critical threshold, the Pop I/II stars form gradually. Therefore, the SFRs of these populations would depend on the hydrogen reionization fraction and pristine fraction, which are shown in Eq (38), Eq (39) and Eq (40). Our results show that the metal enrichment is dominated by “genetic channel” during a large redshift range, leading to the earlier raising of the SFR of Pop II stars, which agrees with the result of Trenti & Stiavelli (2009). However, the upper limit of the metallicity of the metal-enriched region could be larger than that of the galaxies polluted via “genetic channel” due to the inhomogeneous metal pollution of the supernova-driven protogalactic outflows.

For the case of the supernova-driven protogalactic outflow, we make a more reasonable assumption that the SN winds would stall if their pressures are equal to the pressure of IGM, which is different from the previous papers (Furlanetto & Loeb 2005; Greif & Bromm 2006) that calculated the process of the propagation and distribution of metals by assuming that the SN wind propagated for half of the age of the universe via Sedov solution (Furlanetto & Loeb 2005), however, Sedov solution is not well approximated after the SN winds have been stalled by IGM. Our result shows that the IGM is enriched via SN outflows during $z = 4 \sim 10$.

In this paper, we study the NIRB, the SFRs of different populations, and the reionization history simultaneously, which is different from Fernandez & Komatsu (2006) and Cooray et al. (2012a). In previous works, e.g. Cooray et al. (2012a) and Fernandez & Zaroubi (2013), the transition of Pop III to Pop II stars is given by $f_p = (1/2)\{1 + \text{erf}[(z - z_t)/\sigma_p]\}$, where f_p is the fraction of Pop III stars, z_t is the transition redshift and σ_p is the length of the transition. The above equation describing the transition of Pop III to Pop II might be too simple. In fact, the transfer from Pop III to Pop II stars is a very complex process. Here, we consider the some main properties evolution of three stellar populations, such as the metallicity, reionization and star formation rate. Finally, these properties would affect the character of the spectra of NIRB.

As pointed out by Fernandez & Zaroubi (2013), the Ly α bump could reveal information of the Pop III era. Our results show that the Pop III would make a main contribution to the NIRB at high redshift and the spectra of the NIRB might show two bumps due to the different distributions of Pop III.1 and Pop III.2 stars. However, the predicted intensity ($\lesssim 0.2\text{nWm}^{-2}\text{sr}^{-1}$) of NIRB from high redshift ($z > 6$) stars is much lower than the contribution of the foreground ($\sim 10\text{nWm}^{-2}\text{sr}^{-1}$), leading to measuring the signal from high-redshift stars is very difficult. The contributions from low-redshift galaxies and the bright zodiacal foreground should be correctly subtracted. Many works have attempted to measure the excess of NIRB without the contributions of the low-redshift galaxies and other foregrounds (Dwek & Arendt 1998; Gorjian et al. 2000; Kashlinsky & Odenwald 2000; Totani et al. 2001; Wright 2001; Kashlinsky et al. 2002; Magliocchetti et al. 2003; Salvaterra & Ferrara 2003; Cooray & Yoshida 2004; Kashlinsky et al. 2004; Kashlinsky 2005; Matsumoto et al. 2005; Kashlinsky et al. 2007b; Thompson et al. 2007a,b; Cooray et al. 2012b; Kashlinsky et al. 2012). On the other hand, Fernandez & Zaroubi (2013) suggested that we can detect the relative change in the intensity of NIRB, which results from a Lyman α bump as a function of wavelength. However, there are still many ways causing such a change, such as the evolution of the escape fraction or a rapidly changing star formation rate as a function of redshift.

We also calculate the stochastic background of gravitational waves from the collapse of the early stars. However, theoretically, there are several astrophysical sources contributing to the background of gravitational waves, including transient sources (e.g. compact binary coalescence, supernovae, gamma-ray bursts etc.), long-lasting transient sources (e.g. magnetars, long gamma-ray bursts etc.) and continuous sources (e.g. pulsar). Thus it is necessary to distinguish between different sources from the spectrum of gravitational waves. In this paper, we find that it is difficult to observe the SBGWs signals from the early stars, however, for $f_{*,III} \approx 0.01$ and $f_{esc} \approx 0.21$, BBO operating in the range $0.01 - 10\text{Hz}$ might detect lower frequency signal from Pop III.1 stars, which are twice than the sensitivity of BBO.

Acknowledgements

We thank an anonymous referee for valuable and detailed suggestions that have allowed us to improve this manuscript significantly. This work is supported by the National Basic Research Program of China (973 Program, grant No. 2014CB845800) and the National Natural Science Foundation of China (grants 11422325, 11373022, and 11033002), the Excellent Youth Foundation of Jiangsu Province (BK20140016), and the Program for New Century Excellent Talents in University (grant No. NCET-13-0279).

References

- Abel T., Bryan G. L., & Norman M. L., 2002, *Science*, 295, 93
- Planck Collaboration: Ade P. A. R., Aghanim N., Ashdown M., et al., arXiv:1502.01589
- Barkana R., & Loeb A., 2000, *ApJ*, 539, 20
- Barkana R., & Loeb A., 2001, *Phys. Rep.*, 349, 125
- Barlow T. A., & Tytler D., 1998, *AJ*, 115, 1725
- Bouwens R. J., Illingworth G. D., Oesch P. A., et al. 2012a, *ApJ*, 754, 83
- Bouwens R. J., Illingworth G. D., Oesch P. A., et al. 2012b, *ApJ*, 752, L5
- Bromm V., Coppi P. S., & Larson R. B., 1999, *ApJ*, 527, L5
- Bromm V., Ferrara A., Coppi P. S., & Larson R. B., 2001, *MNRAS*, 328, 969
- Bromm V., Coppi P. S., & Larson R. B., 2002, *ApJ*, 564, 23
- Bromm V., & Loeb A., 2003, *Nature*, 425, 812
- Bromm V., & Loeb A., 2004, *New Astron.*, 9, 353
- Bromm V., & Larson R. B., 2004, *ARA&A*, 42, 79
- Bromm V., Yoshida N., Hernquist L., & McKee C. F., 2009, *Nature*, 459, 49
- Bromm V., 2013, *Rep. Prog. Phys.*, 76, 112901
- Bouwens R. J. et al., 2010, *ApJ*, 708, L69
- Buonanno A., Sigl G., Raffelt G. G., Janka H., & Muller E., 2005, *Phys.Rev.D*, 72, 084001
- Carr B. J., 1980, *A&A*, 89, 6
- Cooray A., & Yoshida N., 2004, *MNRAS*, 351, L71
- Cooray A., Bock J. J., Keatin B., Lange A. E., & Matsumoto T., 2004, *ApJ*, 606, 611
- Cooray A., Gong Y., Smidt J., & Santos M. G., 2012a, *ApJ*, 756, 92
- Cooray A. et al., 2012b, *Nat*, 490, 514
- de Souza R. S., Yoshida N., & Ioka K., 2011, *A&A*, 533, 32
- Dwek E., & Arendt R. G., 1998, *ApJ*, 508, L9
- Fan X., Carilli C. L., & Keating B., 2006, *ARA&A*, 44, 415
- Fernandez E. R., & Komatsu E., 2006, *ApJ*, 646, 703
- Fernandez E. R., Komatsu E., Iliev I. T., & Shapiro P. R., 2010, *ApJ*, 710, 1089
- Fernandez E. R., & Shull J. M., 2011, *ApJ*, 731, 20
- Fernandez E. R., Iliev I. T., Komatsu E., & Shapiro P. R., 2012, *ApJ*, 750, 20
- Fernandez E. R., Dole H., & Iliev I. T., 2013, *ApJ*, 764, 56
- Fernandez E. R., & Zaroubi S., 2013, *MNRAS*, 433, 2047
- Ferrara A., 1998, *ApJ*, 499, L7
- Ferrara A., & Tolstoy E., 2000, *MNRAS*, 313, 291
- Ferrara A., Pettini M., & Shchekinov Y., 2000, *MNRAS*, 319, 539
- Franceschini A., Rodighiero G., & Vaccari M., 2008, *A&A*, 487, 837
- Flanagan E. E., 1993, *Phys. Rev. D*, 48, 2389
- Finke J. D., Razzaque S., & Dermer C. D., 2010, *ApJ*, 712, 238
- Furlanetto S. R., & Loeb A., 2005, *ApJ*, 634, 1
- Gilmore R. C., Madau P., Primack J. R., Somerville R. S., & Haardt F., 2009, *MNRAS*, 399, 1694
- Gilmore R. C., Somerville R. S., Primack J. R., & Domínguez A., 2012, *MNRAS*, 422, 3189
- Greif T. H., & Bromm V., 2006, *MNRAS*, 373, 128
- Gorjian V., Wright E. L., & Chary R. R., 2000, *ApJ*, 536, 550
- Hauser G., & Dwek E., 2001, *ARA&A*, 39, 249
- Heger A., & Woosley S. E., 2002, *ApJ*, 567, 532
- Hinshaw G., Larson D., & Komatsu E., et al., 2013, *ApJS*, 208, 19
- Hopkins A. M., & Beacom J. F., 2006, *ApJ*, 651, 142
- Hosokawa T., Omukai K., Yoshida N., & Yorke H. W., 2011, *Science*, 334, 1250
- Hosokawa T., Yoshida N., Omukai K., & Yorke H. W., 2012, *ApJ*, 760, L37
- Inoue Y., Inoue S., Kobayashi M. A. R., et al., 2013, *ApJ*, 768, 197
- Jappsen A.-K., MacLow M.-M., Glover S. C. O., Klessen R. S., & Kitsionas S., 2009a, *ApJ*, 694, 1161
- Jappsen A.-K., Klessen R. S., Glover S. C. O., & MacLow M.-M., 2009b, *ApJ*, 696, 1065
- Johnson J. L., & Bromm V., 2006, *MNRAS*, 366, 247
- Kashlinsky A., & Odenwald S., 2000, *ApJ*, 528, 74
- Kashlinsky A., Odenwald S., Mather J., Skrutskie M. F., & Cutri R. M., 2002, *ApJ*, 579, L53
- Kashlinsky A., Arendt R., Gardner J. P., Mather J. C., & Moseley S. H., 2004, *ApJ*, 608, 1
- Kashlinsky A., 2005, *Phys. Rep.*, 409, 361
- Kashlinsky A., Arendt R. G., Mather J., & Moseley S. H., 2005, *Nat*, 438, 45
- Kashlinsky A., Arendt R. G., Mather J., & Moseley S. H., 2007a, *ApJ*, 654, L1
- Kashlinsky A., Arendt R. G., Mather J., & Moseley S. H., 2007b, *ApJ*, 654, L5
- Kashlinsky A., Arendt R. G., Ashby M. L. N., Fazio G. G., Mather J., & Moseley S. H., 2012, *ApJ*, 753, 63
- Kistler M. D., Yüksel H., Beacom J. F., Hopkins A. M., & Wyithe J. S. B., 2009, *ApJ*, 705, L104
- Kneiske T. M., Bretz T., Mannheim K., & Hartmann D. H., 2004, *A&A*, 413, 807
- Kneiske T. M., & Dole H., 2010, *A&A*, 515, 19
- Komatsu E., Dunkley J., Nolte M. R. et al. 2009, *ApJS*, 180, 330
- Komatsu E., Smith K. M., Dunkley J. et al. 2011, *ApJS*, 192, 18
- Larson R. B., 1998, *MNRAS*, 301, 569
- Lejeune T., & Schaerer D., 2001, *A&A*, 336, 538
- Mackey J., Bromm V., & Hernquist L., 2003, *ApJ*, 586, 1
- MacLow M.-M., & Ferrara A., 1999, *ApJ*, 513, 142
- Madau P., Pozzetti L., & Dickinson M., 1998, *ApJ*, 498, 106
- Madau P., Ferrara A., & Rees M. J., 2001, *ApJ*, 555, 92
- Madau P., & Silk J., 2005, *MNRAS*, 359, L37
- Marassi S., Schneider R., & Ferrari V., 2009, *MNRAS*, 398, 293
- Magliocchetti M., Salvaterra R., & Ferrara A., 2003, *MNRAS*, 342, L25
- Matsumoto T. et al., 2005, *ApJ*, 626, 31
- Múñoz J. A., & Loeb A., 2011, *ApJ*, 729, 99
- Oey Y. M. S., & Clarke C. J., 1997, *MNRAS*, 289, 570
- Ohkubo T., Nomoto K., Umeda H., Yoshida N., & Tsuruta S., 2009 *ApJ*, 706, 1184
- Omukai K., & Palla F., 2001, *ApJ*, 561, L55
- Omukai K., & Palla F., 2003, *ApJ*, 589, 677
- Pereira E. S., & Miranda O. D., 2010, *MNRAS*, 401, 1924
- Portegies Zwart S. F., McMillan S. L. W., & Gieles M., 2010, *ARA&A*, 48, 431
- Press W. H., & Schechter P., 1974, *ApJ*, 187, 425
- Regimbau T., & de Freitas Pacheco J. A., 2006, *ApJ*, 642, 455
- Robertson B. E., Ellis R. S., Dunlop J. S., McLure R. J., & Stark D. P., 2010, *Nat*, 468, 49
- Salpeter E. E., 1955, *ApJ*, 121, 161
- Salvaterra R., & Ferrara A., 2003, *MNRAS*, 339, 973
- Salvaterra R., & Ferrara A., 2006, *MNRAS*, 367, L11
- Sandick P., Olive K. A., Daigne F., & Vangioni E., 2006, *Phys. Rev. D*, 73, 104024
- Santos M. R., Bromm V., & Kamionkowski M., 2002, *MNRAS*, 336, 1082
- Schaerer D., 2002, *A&A*, 382, 28
- Schenker M. A., Robertson B. E., Ellis R. S., et al. 2013, *ApJ*, 768, 196
- Schneider R., Ferrara A., Ciardi B., Ferrari V., & Matarrese S., 2000, *MNRAS*, 317, 385
- Schneider R., Ferrara A., Natarajan P., & Omukai K., 2002, *ApJ*, 571, 30
- Schneider R., Omukai K., Inoue A. K., & Ferrara A., 2006a, *MNRAS*, 369, 1437
- Schneider R., Salvaterra R., Ferrara A., & Ciardi B., 2006b, *MNRAS*, 369, 825
- Stacy A., Greif T. H., & Bromm V., 2012, *MNRAS*, 422, 290
- Stark R. F., & Piran T., 1985, *Phys.Rev.Lett.*, 55, 8
- Stecker F. W., Malkan M. A., & Scully S. T., 2006, *ApJ*, 648, 774
- Suwa Y., Takiwaki T., Kotake K., & Sato K., 2007, *ApJ*, 665, L43
- Tegmark M., Silk J., Rees M. J., et al. 1997, *ApJ*, 474, 1
- Thompson R. I., Eisenstein D., Fan X., Rieke M., & Kennicutt R. C., 2007a, *ApJ*, 657, 669
- Thompson R. I., Eisenstein D., Fan X., Rieke M., & Kennicutt R. C., 2007b, *ApJ*, 666, 658
- Thorne K. P., 1987, in Hawking S. W., Israel W., eds, *Three Hundred Years of Gravitation*. Cambridge Univ. P
- Thrane E., & Romano J. D., 2013, *Phys.Rev.D*, 88, 124032
- Totani T., Yoshii Y., Iwamuro F., Maihara T., & Motohara K., 2001, *ApJ*, 550, L137
- Trenti M., & Stiavelli M., 2009, *ApJ*, 694, 879
- Voit G. M., 1996, *ApJ*, 465, 548
- Wyithe J. S. B., & Loeb A., 2006, *Nat*, 441, 322
- Wang F. Y., 2013, *A&A*, 556, 90
- Wang F. Y., & Dai Z. G., 2009, *MNRAS*, 400, L10
- Wang L., Mao J., Xiang S., & Yuan Y. F., 2009, *A&A*, 494, 817
- Weaver R., McCray R., Castor J., Shapiro P., & Moore R., 1977, *ApJ*, 218, 377
- Wright E. L., 2001, *ApJ*, 553, 538
- Yoshida N., Abel T., Hernquist L., & Sugiyama N. 2003, *ApJ*, 592, 645
- Yoshida N., Oh S. P., Kitayama T. & Hernquist L., 2007, *ApJ*, 663, 687
- Yu Y. W., Cheng K. S., Chu M. C., & Yeung S., 2012, *JCAP*, 7, 23
- Yue B., Ferrara A., Salvaterra R., & Chen X., 2013, *MNRAS*, 431, 383

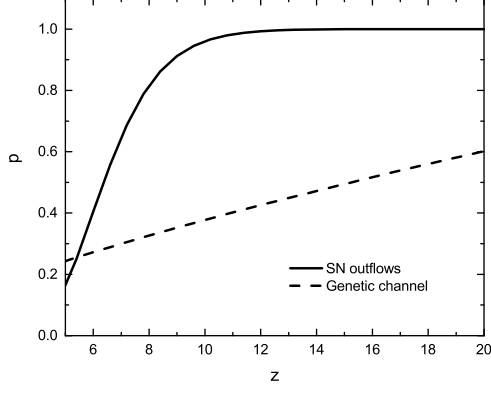


Fig. 1. The evolution of the non-metal fraction. The solid curve corresponds to the evolution of the pristine fraction $p_{pris}(z) = 1 - p_e(z)$, and the dashed curve corresponds to the evolution of $p_{gc}(z)$ that a dark matter halo did not inherit any metals from its progenitor.

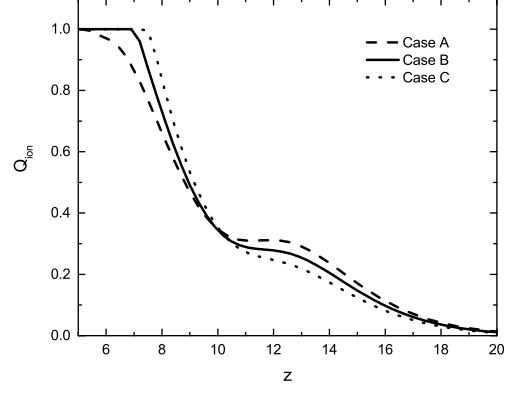


Fig. 3. The hydrogen reionization fraction Q_{ion} as a function of redshift z . Case A ($f_{*,III} = 0.01$, $f_{esc} = 0.21$), Case B ($f_{*,III} = 0.004$, $f_{esc} = 0.45$) and Case C ($f_{*,III} = 0.002$, $f_{esc} = 0.75$) are denoted by dashed, solid and dotted lines, respectively.

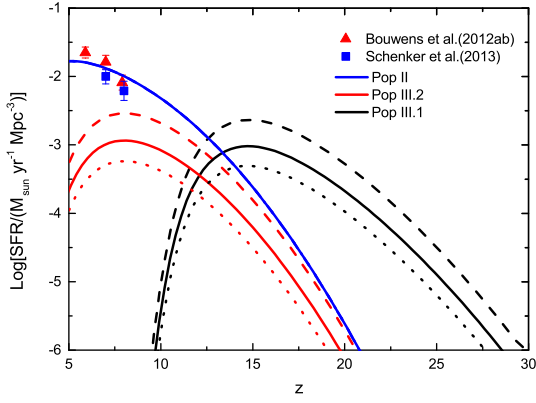


Fig. 2. The three epochs of the cosmic star formation history: the blue line denotes Pop II stars, the black line denotes Pop III.1 stars, and the red line denotes Pop III.2 stars. Case A ($f_{*,III} = 0.01$, $f_{esc} = 0.21$), Case B ($f_{*,III} = 0.004$, $f_{esc} = 0.45$) and Case C ($f_{*,III} = 0.002$, $f_{esc} = 0.75$) are denoted by dashed, solid and dotted lines, respectively. The observed data is given by Bouwens et al. (2012a,b) and Schenker et al. (2013)

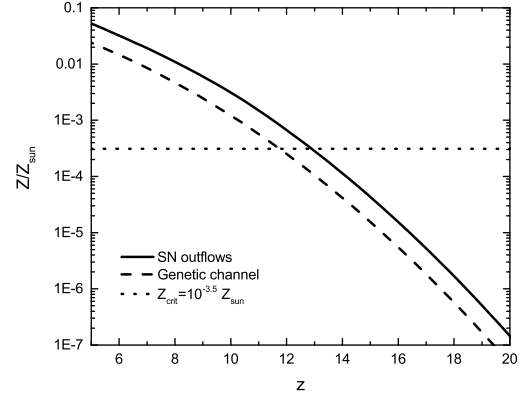


Fig. 4. The evolution of the upper limit of the metallicity. The solid line denotes the upper limit of the metallicity in the metal-enriched region of IGM. The dashed line denotes the upper limit of the metallicity in the galaxies whose all progenitors were polluted via “genetic channel”. The dotted line denotes the critical metallicity $Z_{crit} = 10^{-3.5} Z_{\odot}$.

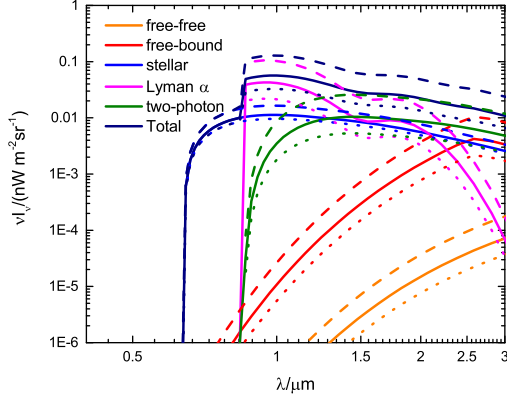


Fig. 5. The spectra of NIRB at redshift $z > 6$. Case A ($f_{*,III} = 0.01, f_{esc} = 0.21$), Case B ($f_{*,III} = 0.004, f_{esc} = 0.45$) and Case C ($f_{*,III} = 0.002, f_{esc} = 0.75$) are denoted by dashed, solid and dotted lines, respectively. Different color lines denote different contributions to the emission of NIRB.

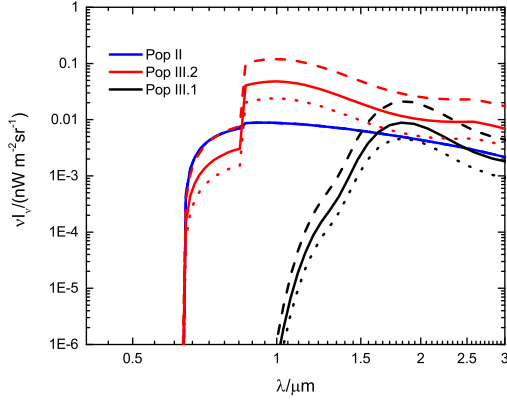


Fig. 6. The contributions of the different stellar populations to NIRB. The blue, black and red lines denote the NIRB contribution of Pop II, Pop III.1 and Pop III.2, respectively. Case B ($f_{*,III} = 0.004, f_{esc} = 0.45$) and Case C ($f_{*,III} = 0.002, f_{esc} = 0.75$) are denoted by dashed, solid and dotted lines, respectively.

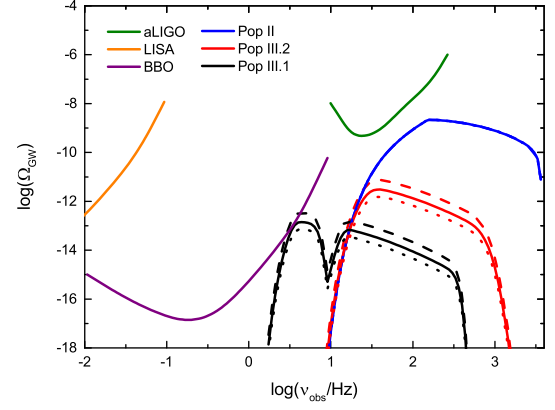


Fig. 7. The spectrum of the gravitational waves. Pop II, Pop III.2 and Pop III.1 stars are denoted by blue, red, and black lines, respectively. Case B ($f_{*,III} = 0.004, f_{esc} = 0.45$) and Case C ($f_{*,III} = 0.002, f_{esc} = 0.75$) are denoted by dashed, solid and dotted lines, respectively. The sensitivity curves of advanced LIGO H1L1, LISA and BBO are denoted by green, orange and purple, respectively (Thrane & Romano 2013), assuming $T = 1$ yr of observation.